Nuclear Instruments and Methods in Physics Research A 597 (2008) 257–265

Contents lists available at ScienceDirect

Nuclear Instruments and Methods in Physics Research A

journal homepage: www.elsevier.com/locate/nima

Gas Electron Multiplying Detectors for medical applications

Edward Tsyganov [a,*], Peter Antich [a], Robert Parkey [a], Serguei Seliounine [a], Viacheslav Golovatyuk [b], Sergey Lobastov [b], Valeriy Zhezher [b], Alexei Buzulutskov [c]

[a] The University of Texas, Southwestern Medical Center, 5323 Harry Hines Blvd., Dallas, TX 75390-9071, USA
[b] Joint Institute for Nuclear Research, Dubna, Russian Federation
[c] Budker Institute of Nuclear Research, Novosibirsk, Russian Federation

ARTICLE INFO

Article history:
Received 21 May 2008
Received in revised form
10 September 2008
Accepted 15 September 2008
Available online 25 September 2008

Keywords:
Gas Electron Multiplying Detectors
Computed Tomography
Single-Photon Emission Tomography

ABSTRACT

The present work describes the development of a new detection technology for medical imaging using the method of Single-Photon Emitted Computed Tomography (SPECT) combined with X-rays Computed Tomography (CT). Our ultimate goal is to advance disease detection by imaging quantitatively molecular agents and localizing their distribution in tissues and organs by SPECT simultaneously with the anatomical CT image. To assess the imaging characteristics of the imaging agents developed, we tested and advanced a detection technique first developed for high-energy physics: Gas Electron Multipliers (GEMs).

1. Introduction

Gas Electron Multiplier (GEM) detectors are micro-patterned gas detectors, consisting of thin (50 μm) insulating foils, metal-clad on both sides, and perforated with a high-density matrix of holes with micrometer-sized diameters. The detection of photons occurs in these detectors by the interaction of recoil electrons with the gas and amplification of the signal under the potential difference applied between the metal electrodes [1]. The use of chemically inert noble gases circumvents decomposition under avalanche conditions, and thus makes possible long-term operation of sealed modules, a factor which is of primary importance in the development of practical devices. The operation of several GEMs in tandem (in cascade) [2,3] is a unique feature of this technology making it possible to achieve amplification factors exceeding 10^6 [3]. Photon and ion feedback suppression substantially improve the multi-GEM operation when equipped with ultraviolet (UV) and visible photocathodes; and considerably reduces the aging rate of the photocathode under avalanching, thus increasing the lifetime of the device [4–7].

This study provides the information necessary for the construction of clinical and preclinical imaging devices, based on a quantitative dual-modality Single-Photon Emitted Computed Tomography (SPECT)–Computed Tomography (CT) scanner combining anatomic and biomarker information to improve diagnosis and determine the time course of the disease in treated patients, thus providing fast and reliable guidance for the treatment. The quantitative dual-modality SPECT–CT scanner is a crucial instrument for a breakthrough in breast cancer diagnostics and follow-up therapy, and could drastically reduce false diagnoses, and provide fast and reliable guidance for healing.

The high spatial and energy resolution of GEM detectors will make it possible to distinguish different radio-markers in small volumes. It will allow the location of cancer cells by targeting with isotopes with a different energy of illuminating photons.

Current research in molecular imaging, in particular using SPECT and Positron Emission Tomography (PET), focuses on disease-specific targets and searches for molecular biomarkers. In parallel there is a continuing interest in the use of anatomic imaging for the detection of small structures (e.g. trabecular architecture in bone, small tumors in cancer, and vascular architecture). These twin foci of interest imply heightened requirements in spatial and temporal resolution, so that for dual-mode imaging it may become possible to precisely locate the biomarker's location and characterize its biodistribution as it changes in space and time.

A potential tool for supporting these methods is a promising new GEM technology for digital detection of gamma- and X-rays, which we are currently testing for medical applications. This technology is both useful for the detection of very low radiation levels and necessary for effective performance in the single-photon counting mode.

The two modes of medical imaging on which we focus in this research, CT and SPECT, benefit from high spatial and temporal

* Corresponding author.
E-mail address: edward.tsyganov@utsouthwestern.edu (E. Tsyganov).

0168-9002/$ - see front matter © 2008 Elsevier B.V. All rights reserved.
doi:10.1016/j.nima.2008.09.002

resolution combined with digital readout and the capability of detecting single photons with high efficiency. The precise energy measurement in CT scans allows the use of a multiple-energy scans to characterize tissues and enhance anatomic tissue contrast, while in SPECT dual/triple isotope imaging becomes feasible. Tracers with ^{125}I could be imaged at 1 bar gas pressure and ^{99m}Tc tracers may be imaged at 5 bar with the same detector. Dual/triple tracer SPECT scanning becomes possible due to high energy resolution of GEM detectors.

The significance of the work is that a new imaging modality would derive from it, specialized for pendant breast cancer SPECT–CT imaging and capable of merging very precise high-contrast anatomic imaging with quantitative, high-sensitivity molecular imaging.

2. Methods

GEM devices exploit the ionization released in a gas to multiply photoelectrons in dielectric sheets covered with metal electrodes and perforated with microchannels in which the photoelectrons accelerate and multiply. Kapton-based GEMs produced in planar or cylindrical forms are technically feasible and economical. The major technical advantages of GEM-based devices operated in Xe or Ar, when compared to the crystals readout by vacuum Photomultipliers (PMTs), are (1) the solution of the parallax problem, thus better resolution; (2) a better spatial resolution; and (3) a lower cost.

Hence, the application of GEM to digital imaging systems could improve performance in digital mammography, as compared to present techniques, by offering much lower noise, a wider dynamic range, and improved contrast resolution. A GEM-based detector can compete with large-area flat-panel Si imaging devices, intensively developed in the past few years. One of the advantages of a GEM-based detector, in addition to the lower cost, robust digital readout, and fine spatial resolution, would be its ability to work in the nuclear medicine mode with energy measurement.

The optical readout of GEMs was first studied using a charge-coupled device (CCD) camera [8] with which the light emissions and localization properties of GEMs were studied for neutron detection. The two-dimensional electronic readout with a high spatial resolution (40 μm) [9–11] and various readout structures (orthogonal, stereo) were successfully implemented, and the sensitive area varied from 10×10 to $40\times40\,cm^2$. With up to 3 bar of gas pressure GEMs achieved enhanced sensitivity [12] while maintaining the high gain obtained in triple-GEM structures.

3. Test results

We built and tested a prototype GEM chamber $10\times10\,cm^2$ in size [9] (Fig. 1).

This is a triple-GEM structure. Fig. 2 shows the GEM device opened to show the components and its installation on a mammography device.

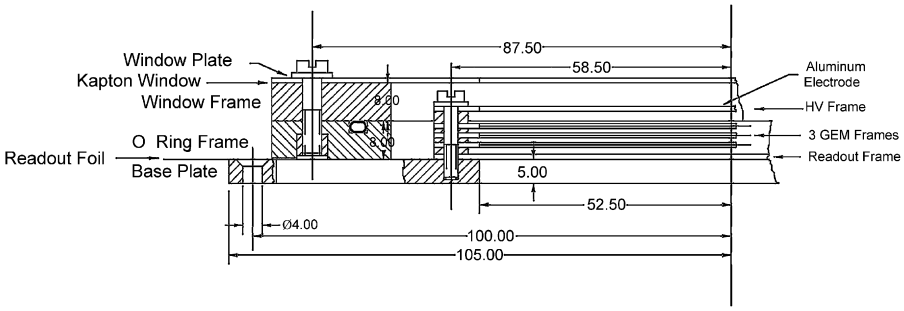

Fig. 1. Schematic drawing of the prototype 3-GEM structure built in Dallas.

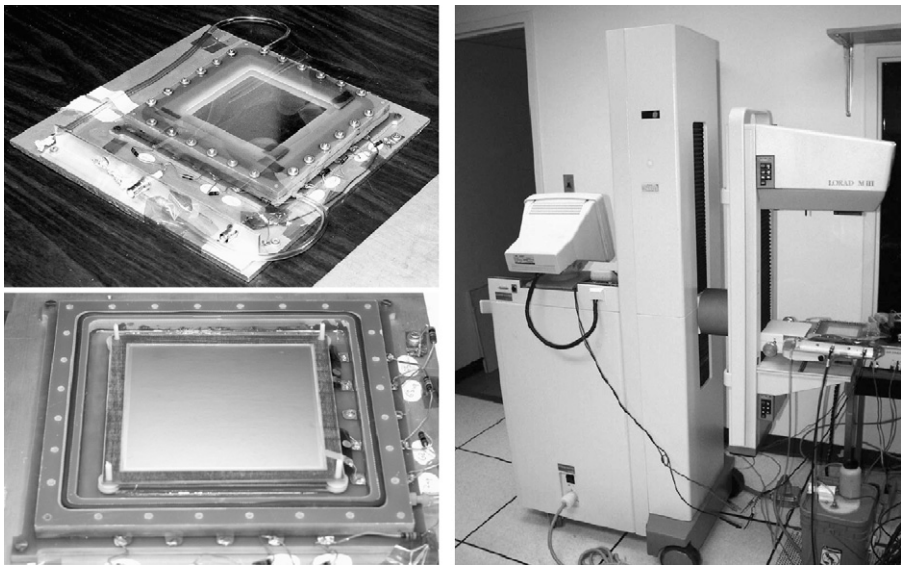

Fig. 2. Left—two views of the initial GEM chamber, assembled and open to show the GEM electrode. Right—GEM Chamber positioned in a LORAD M III, GE mammography unit.

We used a gas mixture of Ar/CO_2 in a ratio of 95/5. Soft X-rays from a clinical mammography unit (LORAD M III, GE) with a molybdenum target irradiated the chamber.

Proof of principle images were obtained with a simple CCD camera. The digital imaging camera incorporates a Texas Instruments TC245 CCD image sensor that is sensitive to light from the blue to the infrared range. This is a black-and-white frame transfer CCD, with an image area of 786 (H) × 488 (V) pixels. The CCD has a high dynamic range (more than 70 dB), high sensitivity, high photoresponse uniformity, and low dark current.

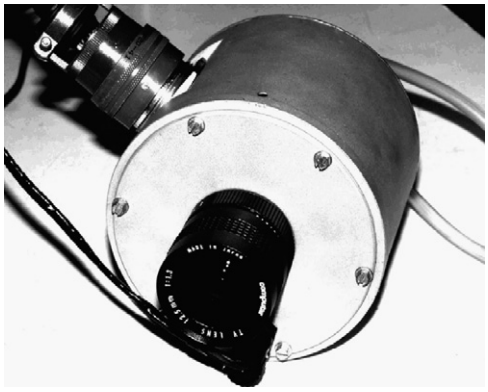

Fig. 3. CCD camera used in the experiment.

The camera head consists of the CCD chip, a fixed focal optical lens with a 1.3 f-number, a two-stage Peltier element affixed to a cold plate, and a heat exchanger. The cooling system uses 10 °C water to cool the Peltier element, which in turn cools the CCD to −25 °C in order to minimize the dark current, and thus the noise in the image. A digital image of 252 (H) × 242 (V) pixels is produced by binning the adjacent pixels in order to improve the signal-to-noise ratio for low-light imaging. The CCD controller produces all the signals necessary to operate the chip, it also processes and digitizes (12 bit) its output signals and communicates with the personal computer for image capture and storage. Fig. 3 presents a general view of the device. Fig. 4 presents some images obtained during the experiment.

The spatial FWHM resolution was estimated to be about 0.5 mm, and we believe that improvements in the readout and other technical characteristics resulting from this study could further improve the resolution.

4. Energy measurements

To measure photon energy resolution, we tested the triple-GEM chamber with a readout electrode of $9 \times 9\,cm^2$ area, placed within 4 mm of the last GEM electrode to collect the charge

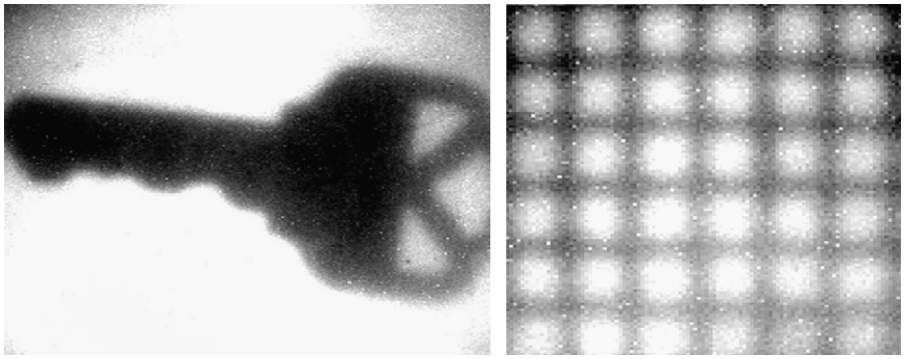

Fig. 4. Left—image of a key. Right—image of a 2 mm grid. KVp is 19 kV in both cases.

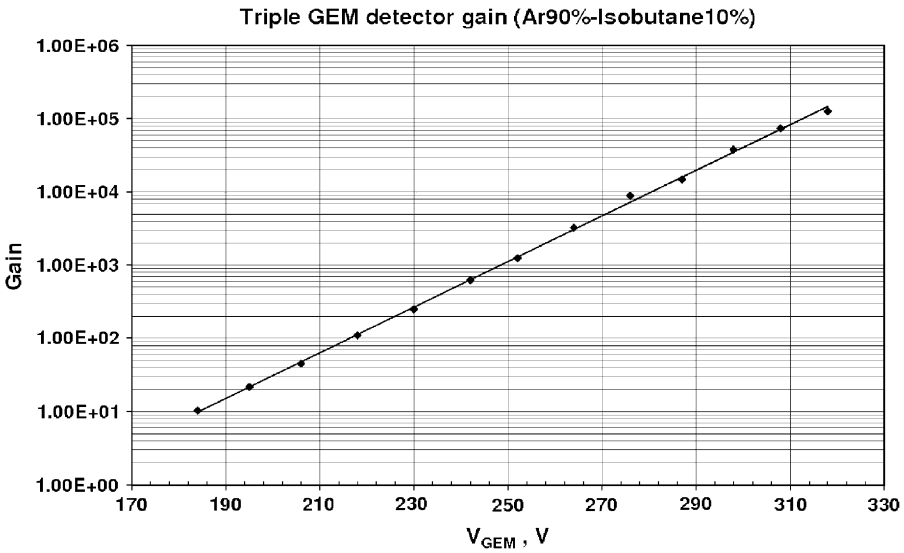

Fig. 5. Gain of the triple-GEM chamber with a gas mixture of Ar and isobutane in a 90/10 ratio versus voltage on each GEM. The first nine points were measured using the X-ray flux from the mammography unit with a molybdenum target, and the last four points using a ^{55}Fe source. A single exponential line interpolates the data points.

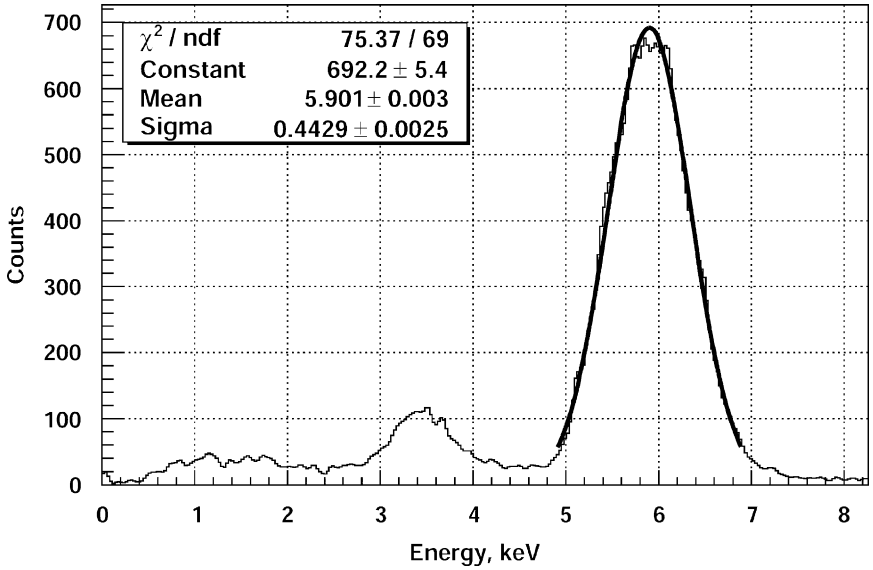

Fig. 6. Energy spectrum obtained when the chamber was irradiated with ^{55}Fe. The main peak is fitted with Gaussian, FWHM is 18%. The escape peak is clearly visible. The trigger threshold was equivalent to about 0.5 keV.

produced by gamma-rays from radioactive sources after amplification. The electrode signal was then amplified by a further factor of 100 in a Phillips Scientific Model 6931, 100 MHz bipolar amplifier, and read by a LeCroy 2248A ADC which integrates the charge over 200 ns, a time appropriate for the processes involved. Initially, we used a gas mixture of argon–isobutane in a proportion 90%/10%. At a GEM voltage of 315 V, the gain of the chamber was 1.2×10^5.

To measure the gain at high voltages, the chamber was irradiated with a ^{55}Fe radioactive source. An average ionization energy 26 eV is spent in Ar and 23 eV is spent in isobutane to produce one electron–ion pair [13]; therefore, we know the initial charge after photoabsorption in the drift gap. Our electronics were charge calibrated; therefore, we know the chamber gain.

The gain is high, and varies with voltage (Fig. 5).

We then measured the energy spectra both in argon and xenon from ^{55}Fe and ^{125}I.

The measured energy spectrum from ^{55}Fe for the argon–isobutane mixture is presented in Fig. 6. FWHM energy resolution is 18%, good for such small energy and defined predominantly by the ionization clusters statistics. Measured FWHM noise, including the chamber and our analogous electronics, was less than 70 eV.

The measured energy spectrum with ^{125}I radioactive source when a gas mixture of Ar and isobutane in a 90–10% ratio was used, is presented in Fig. 7. The main peak at 27 keV is not well pronounced because an electron after photoabsorption has a range of about 2 mm and often escapes the 4 mm drift gap. The peak at 8 keV is probably due to fluorescent X-rays from our thick copper-plated electrode. Such signals should be rejected because they did not carry coordinate information.

To detect ^{125}I efficiently, Xe gas could be used instead of Ar. Fig. 8 presents the linear attenuation coefficients for gaseous Xe. The detection efficiency for ^{125}I is more than 5%/cm. The density of Xe at STP is 5.86 g/l, in comparison with 1.78 g/l for Ar, more than three times larger; therefore, the range of the photoabsorption electrons decreases correspondingly [13]. This is important for correct energy and coordinates measurements.

Fig. 9 presents the energy spectrum for ^{125}I when the chamber was filled with a Xe–isobutane (90:10) gas mixture. This time 27 keV peak is well pronounced. Two more low-energy peaks are probably due to X-ray fluorescence in copper from the readout

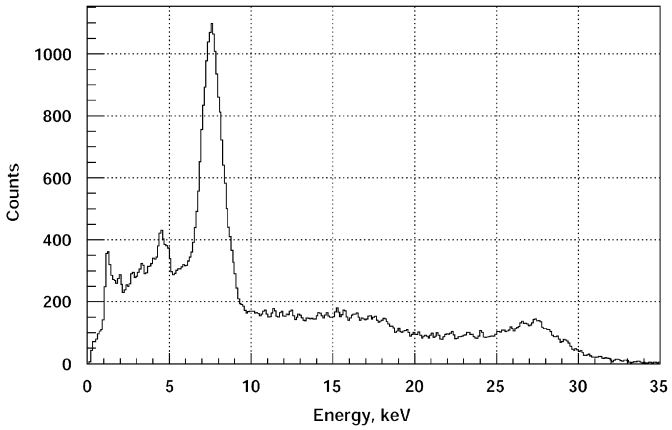

Fig. 7. Energy spectrum obtained when the chamber was irradiated with a ^{125}I source.

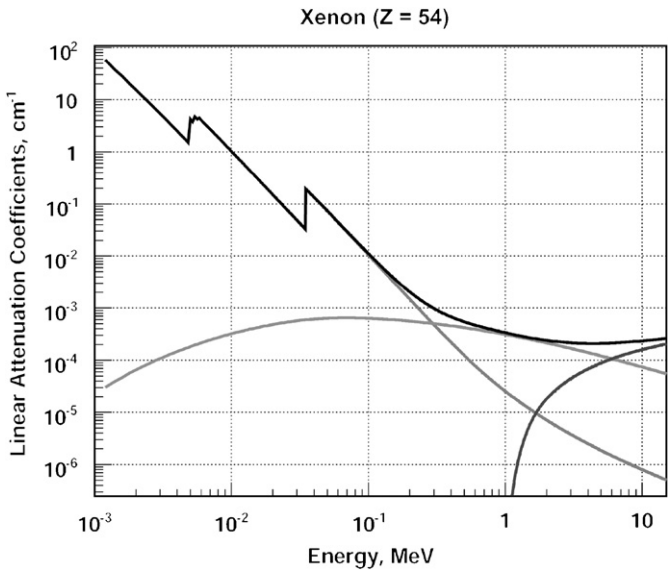

Fig. 8. Linear attenuation coefficients for gaseous Xe at atmospheric pressure.

board and in xenon outside of the sensitive gap. The voltage on GEM electrodes was 390 V, and the gain of the system was about 1.2×10^4. To calculate the gain, the average ionization loss in xenon was taken equal to 22 eV [13]. Fig. 10 shows a typical signal pulse from the ^{125}I source. The width of the pulse is defined by the size of the electron cluster and a drift velocity in the drift gap.

In the case of higher energy isotopes, such as ^{99m}Tc, pressurized GEM chamber should be used. A wider drift gap could also be used, although a parallax problem appears. The ultimate solution of the parallax problem is a direct determination of the *Z*-coordinate (across the drift gap) of the X-ray conversion point. This can be achieved by measuring the drift time of the primary ionization cluster from the conversion point to the first GEM. To accurately measure the time, a "start" signal is needed. For this purpose we intend to use the scintillation signal induced by primary ionization in Xe gas, recorded with the help of a CsI photocathode deposited on the first electrode of the first GEM gap [14]. The CsI photocathode is known to be stable in such gas media and to have high quantum efficiency in the emission region

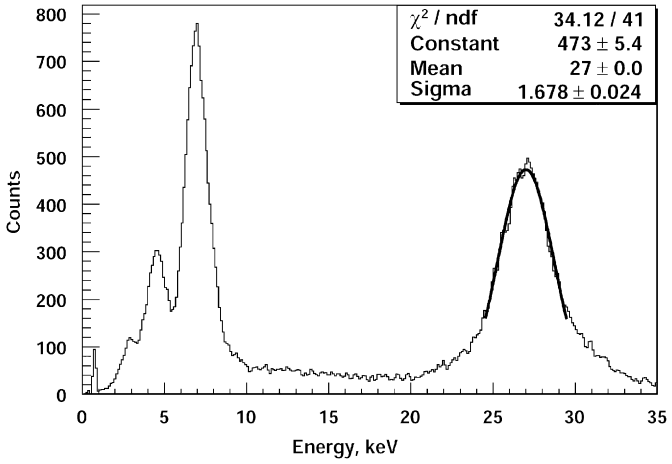

Fig. 9. Energy spectrum for the ^{125}I source in a Xe–isobutane (90:10) gas mixture. The 27 keV peak is well pronounced. Two more low-energy peaks are probably due to X-ray fluorescence in copper from the readout board and in xenon outside of the sensitive gap. The FWHM energy resolution for ^{125}I is about 14%.

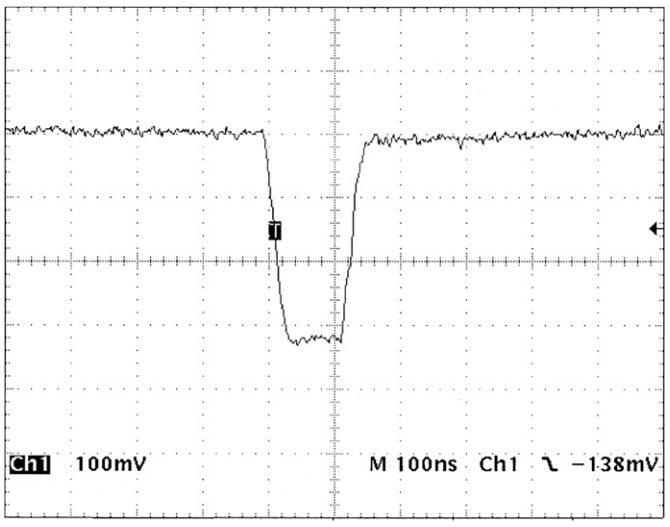

Fig. 10. A typical signal pulse of ^{125}I gamma in a Xe–isobutane (90:10) mixture. The near flat-bottom shape of the pulse illustrates a size of about 25 keV for the electron cluster.

of Xe. The "start" signal would then be followed by a charge signal at a time $(z-d)/v_d$, where d is the gap thickness and v_d is the electron drift velocity. Once the parallax problem is solved, the drift gap thickness and consequently the X-ray detection efficiency can be significantly increased. In the case of a 5-bar pressure and 10-cm drift gap, ^{99m}Tc photon detection efficiency reaches to about 20%.

5. Monte Carlo simulation

5.1. X-ray imaging

A simulation of GEM detector performance in X-ray imaging was done using the Geant4 detector simulation toolkit [15]. X-rays with a mean energy of 30 keV and Gaussian energy distribution with a standard deviation σ 10 keV were emitted from a point-like source uniformly within a cone. Such energy distribution is approximately equivalent to 60 kVp with a 4 mm aluminum filter. The center of a phantom (a sphere with a 10 cm diameter filled with water) was placed 50 cm from the X-ray source. In the middle of the phantom, two small spheres 3 mm in diameter were, one filled with aluminum ($Z = 13$, density 2.70 g/cm^3) and the other filled with calcium ($Z = 20$, density 1.55 g/cm^3) were placed. The distance between the centers of the later spheres was 13 mm. The face of the xenon-filled $1 \times 15 \times 15$ cm^3 detector was located 15 cm upstream from the center of the phantom. The "world" was filled with an air.

The PENELOPE low-energy electromagnetic interaction model within the Geant4 [16] was used to simulate the interaction of the X-rays with the matter. Each X-ray that reached the detector was counted as an event, independent of its energy measured by the detector. The energy resolution of the detector was simulated to be about 10% (FWHM), and the position R.M.S. resolution in the detector was 0.2 mm. In the simulation, detector efficiency was taken 100% (i.e. the efficiency correction presumed to be made).

Some results of the simulation are presented. Fig. 11 illustrates the two-dimensional distribution of the detected events. One-dimensional histograms of the events within a 1-mm central strip in the *Y*-direction are presented in Fig. 12. Fig. 12 (left) presents events selected in the energy range from 25 to 30 keV, and Fig. 12

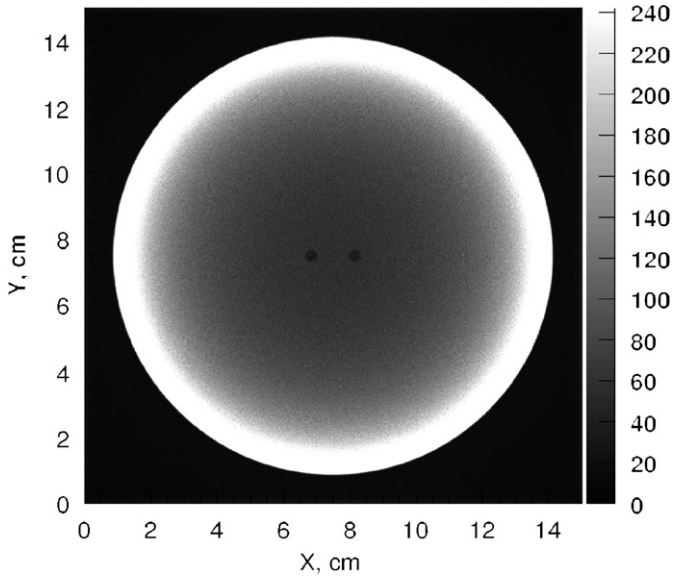

Fig. 11. Two-dimensional distribution of the detected events. All events are presented.

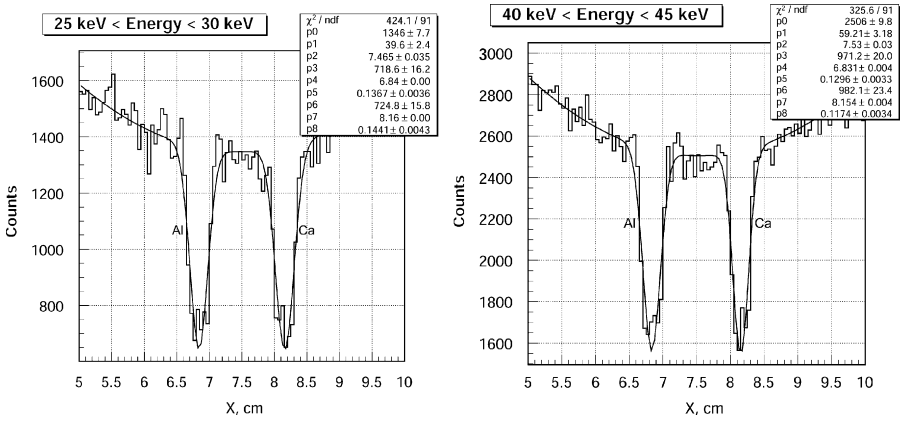

Fig. 12. Left—one-dimensional distribution of the events through the central *Y*-strip of 1 mm wide for the energy range from 25 to 30 keV. The ratio of the Ca signal to the water is about 0.54. Right—distribution of the events through the central *Y*-strip 1 mm wide for the energy range from 40 to 45 keV. The ratio of the Ca signal to the water is about 0.39.

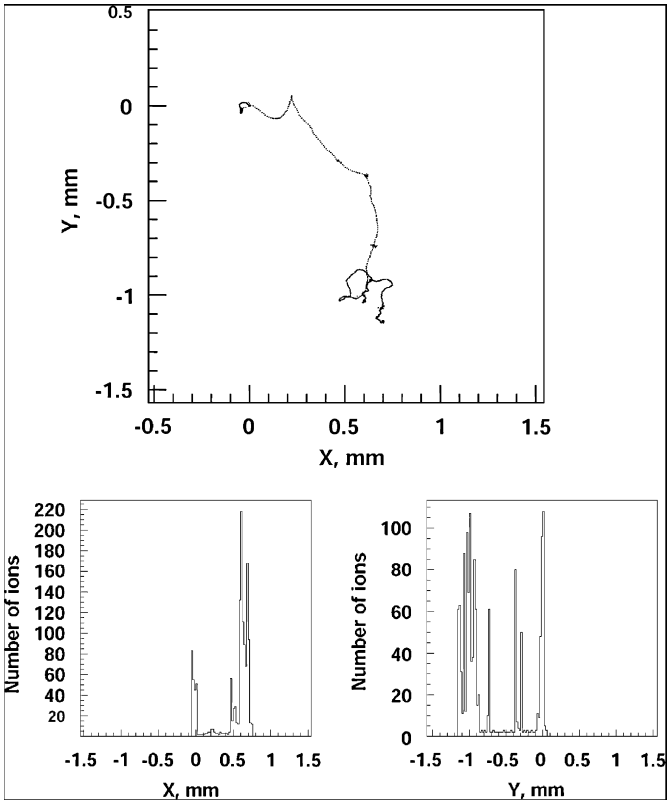

Fig. 13. A typical Monte Carlo event of 30 keV photon absorption in Xe at 1 bar. Photoabsorption occurred at $X = Y = 0$. Upper panel—*X*–*Y* graph of ionization electrons. Lower panel—distributions of ionization in the *X* and *Y* directions.

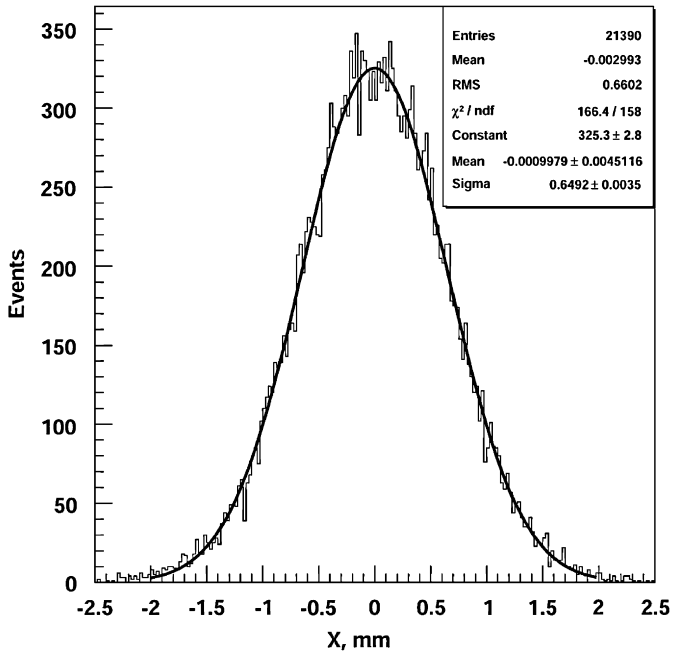

Fig. 14. Spatial resolution of GEM detector with Xe gas at 1 bar for 30 keV photons obtained using the center of gravity (baricenter). FWHM is about 1.5 mm.

(right) presents events selected in the energy range from 40 to 45 keV. The data are fitted with a parabola and two Gaussians. The ratio of Ca signal to the water background is 0.54 for the 25–30 keV range, and 0.39 for the 40–45 keV range.

5.2. Spatial resolution

We investigated the possible lowest limit of spatial resolution for the GEM chamber detecting *x*- or *y*-rays. We assume readout electronics with a noise level less than a signal from one electron in a GEM gap, and an unlimited pitch size. In practice, such a noise level of the order of 10^5–10^6 electrons on the readout input is quite achievable, and pitch size of 0.2 mm or less could be considered as "unlimited." We also ignore a smearing of signal in GEM structure.

We simulated absorption of photons in a Xe gas at normal pressure and temperature; the resulting photoelectrons were slowed down with the ionization process. In order to trace electrons with multiple scattering and ionization, the PENELOPE low-energy electromagnetic interaction model within Geant4 [16] was used.

Two distinct cases of gamma energies were considered in simulation, namely 30 and 40 keV. The 30 keV case is considered as a typical for SPECT with ^{125}I, and the 40 keV is considered as an example for X-ray imaging. In xenon, for the case of 30 keV photons, the K-shell is unavailable for the total absorption process. On the contrary, for 40 keV the K-shell is the major player in the process.

First, let us consider in detail the case of 30 keV.

We are aware that the existing program was capable of tracing the electrons in the gas until the energy loss exceeds 100 eV. In such an approximation, the program produces only about 26 secondary electrons after the 30 keV gammas were absorbed. For a more precise description of the process, one has to know the cross-sections of ionization and the excitation of atoms in the filled gas by electrons up to a very low energy.

We decided to overcome the problem with some technical tricks. We chose a track simulation with steps as small as 1 μm and summed up the averaged energy loss in each step. When the sum reaches the value equal to the average ionization energy in the considered case (22 eV), the program suggests that an act of ionization took place.

On the upper plot of Fig. 13, a typical case of an electron track which was created by a 30 keV photon in Xe is presented. The

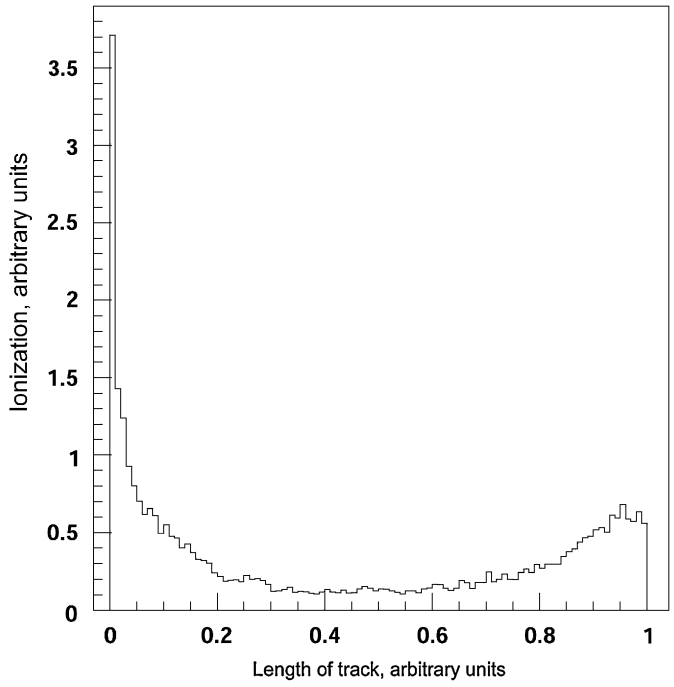

Fig. 15. Ionization along the track for the events that extended predominantly along one of the axes. The events were selected when one projection length is larger than the other by more than a factor of 4. The length of the projection is then normalized for the actual length of the track projection. Sharp peak at the beginning of the track is due to Auger electrons.

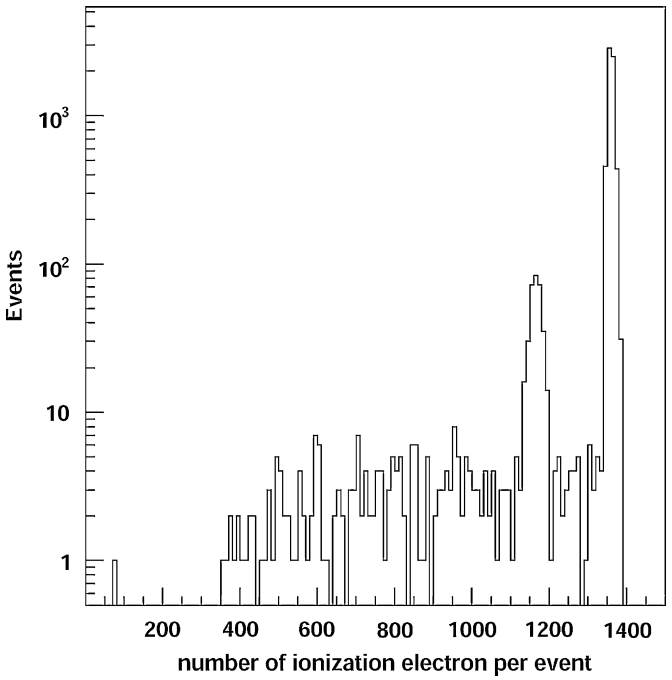

Fig. 17. Ionization detected in a fiducial volume $5 \times 5 \times 5\,\mathrm{mm}^3$. Right peak—full energy deposition. Left peak—secondary photons at 4–5 keV escape the fiducial volume.

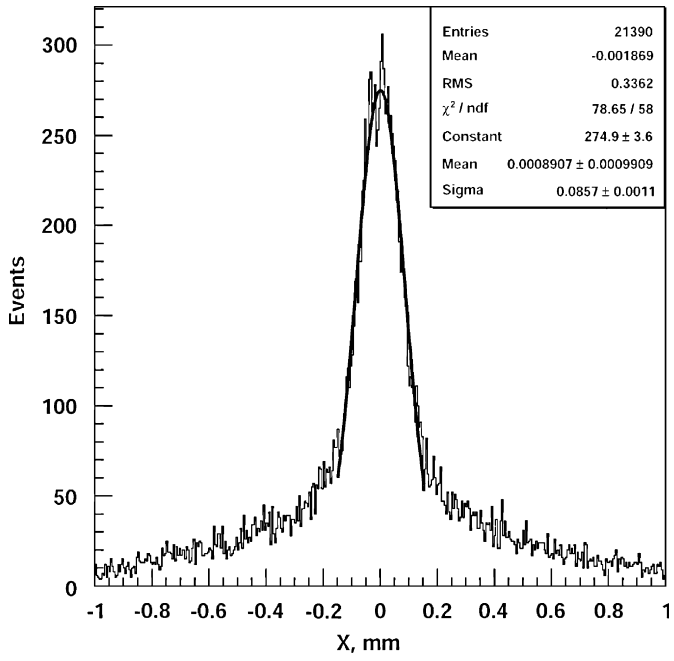

Fig. 16. Spatial resolution in Xe gas at 1 bar, using identification of the origin and the end sides of the electron track. FWHM is about 0.2 mm.

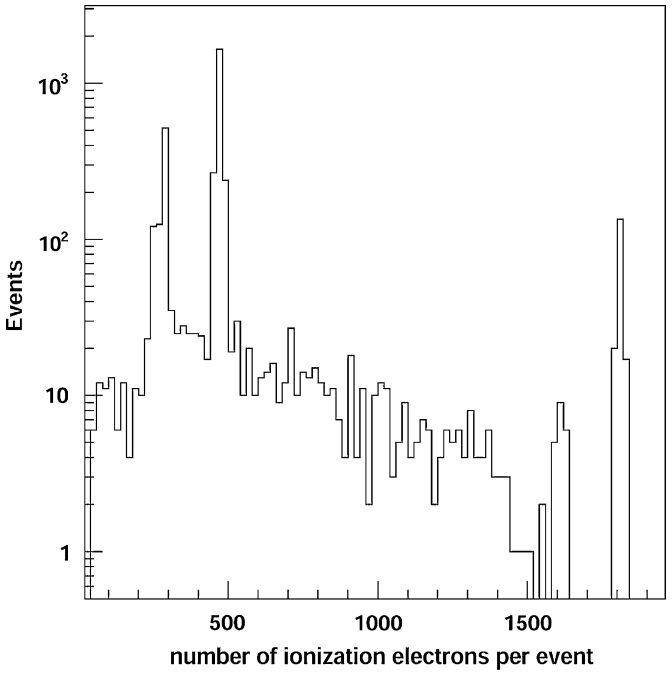

Fig. 18. Ionization released within a fiducial volume of $3 \times 3 \times 3\,\mathrm{mm}^3$ around the interaction point in Xe in the case of a 40 keV photon.

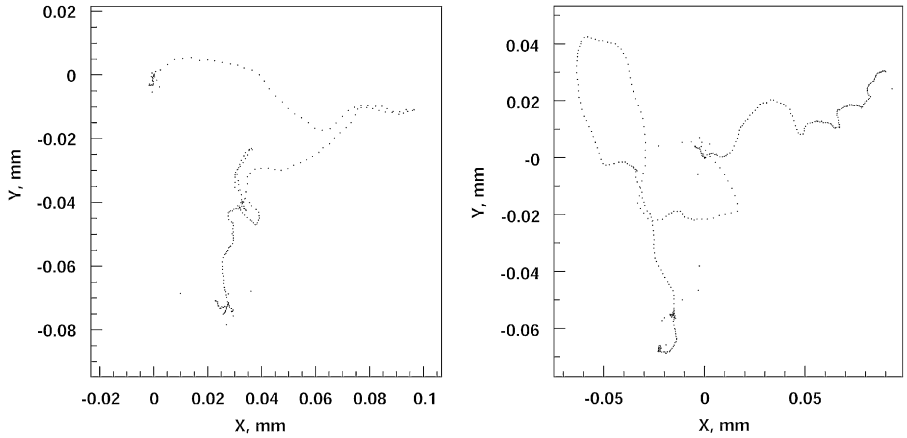

Fig. 19. Cases of an electron tracks after the interaction of 40 keV photons with Xe in the vicinity of the interaction. On the right side image, more than one electron was generated due to atomic relaxation.

distributions of the ionization in both the *X* and *Y* directions are presented in the lower panel of Fig. 13. The peaks in the distributions represent ionization clusters produced along the energetic secondary electrons. All the atom relaxation processes are treated in PENELOPE in great details. Auger electrons are the distinctive feature of the process [17].

If the readout system consists of strips with a fine pitch, one may get the charge distribution in both *X* and *Y* projections. The simplest way to define the position of photoabsorption is by measuring the center of gravity (baricenter) of the considered distributions. Fig. 14 presents the results of such calculations.

During our analysis, we observed that the ionization clusters (fluctuations or "flushes") typically occur first at the beginning of the track, as a result of the relaxation processes of the atom after the photoabsorption, and then at the end of the electron range. High frequency of "flushes" at the end of the track reminds a heavy particles Bragg's ionization peak, but this time for electrons. Fig. 15 demonstrates ionization versus range for the photoabsorption events that extended predominantly along one of the axes. For this graph the events were selected if one projection length is larger than the other by more than a factor of 4.

Using these features, it is possible in most cases to identify the origin of a track (the impact point) and its end side, and thereby improve the spatial resolution. The results of a simple algorithm are presented in Fig. 16. The origin and end of the track are not correctly identified in all the events, but an improvement in spatial resolution is obvious. In the case of *X*, *U*, and *V*, even greater readout improvements in spatial resolution are possible as a result.

Bellazzini et al. [18] used a finely subdivided Gas Pixel Detector based on GEM technology to derive the impact point of very soft X-rays. Our attitude is in the line with the approach of Ref. [18].

It should be noted that such an approach to the coordinate reconstruction will work better when x- or y-ray energy increases, in contrast to the center of gravity (baricenter) method.

At 30 keV, photoabsorption in Xe happens predominantly on the L-shell. Secondary fluorescent photons with energies in the range of 4–5 keV escape the atom and have an average range to the interaction of about 4 mm in Xe gas at 1 bar.

Fig. 17 presents the distribution of the number of ionization electrons per event in a fiducial volume of $5 \times 5 \times 5\,\mathrm{mm}^3$ around the interaction point. In this case, many of the fluorescent photons interact within the fiducial volume and are integrated in the full energy peak.

Now, let us consider the case of a 40 keV photon. In this case, more than 90% of the total absorption processes involve K-shell electrons. Fig. 18 presents ionization released within a fiducial volume of $3 \times 3 \times 3\,\mathrm{mm}^3$ around the interaction point.

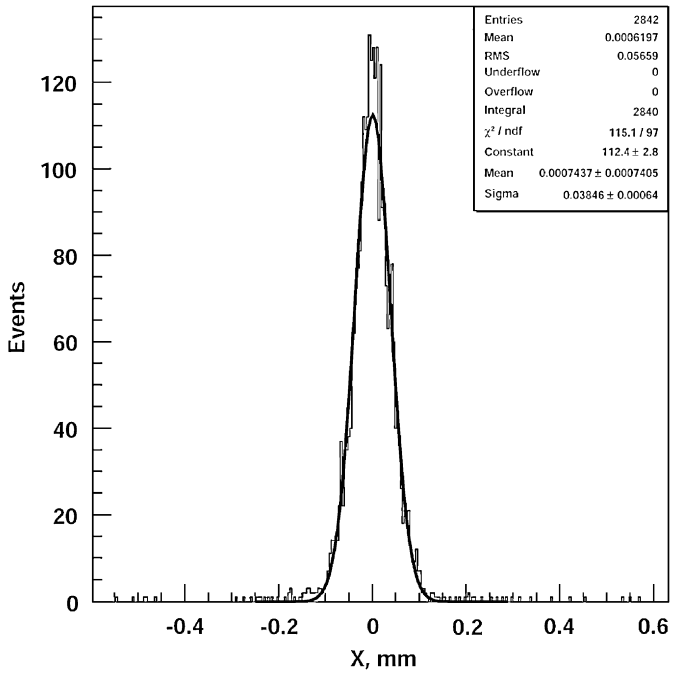

Fig. 20. Spatial resolution for 40 keV photon interactions in Xe obtained using the center of gravity, when only the clusters with less than 500 electrons of ionization are selected for analysis. FWHM is about 0.1 mm.

According to Fig. 18, atomic relaxation produces less than a 10 keV energy release (500 electrons of ionization) in the vicinity of the interaction point, and about 30 keV escapes the vicinity of the interaction point, probably due to a photon emitted after L–K transition. Two distinct cases of such events are presented in Fig. 19.

Fig. 20 shows the spatial resolution of 40 keV photon detection when only the clusters with less than 500 electrons of ionization are selected for analysis using the center of gravity. Because escaping 30 keV photons have a rather large free path in gaseous Xe, a separation of clusters looks easy. In this case, 5-bar Xe pressure would be preferable for the detection of the full energy absorption.

6. Discussion

An important advantage of the electronic readout option is the real possibility of measuring energy. Using this option, the digital readout can be used for background rejection and to implement a "dual energy" scan. The energy resolution of GEM detectors would be of the order of 10–15% [5]. This would allow further improvement of the image contrast.

The preliminary results of the Monte Carlo simulations of X-ray detection by GEM detectors support our hypothesis that the contrast of an image could be optimized with the energy selection of the detected events. These simulations also suggest that FWHM spatial resolution of 0.2 mm is achievable in principal for a ^{125}I source. For X-rays with energy over 35 keV, comparable spatial resolution is achievable, with separation of vicinity and escape clusters.

Acknowledgments

We would like to thank Prof. F. Sauli of CERN for the invaluable help during the GEM design and building phase. We are grateful to Dr. L. Ropelewski and Dr. N. Malakhov of CERN for their discussion of the electronic readout schemes.

References

[1] F. Sauli, Nucl. Instr. and Meth. A 386 (1997) 531.
[2] A. Bachmann, A. Bressan, L. Ropelewski, F. Sauli, A. Sharma, D. Mormann, Nucl. Instr. and Meth. A 438 (2000) 376.
[3] A. Buzulutskov, A. Breskin, R. Chechik, G. Garty, F. Sauli, L. Shekhtman, Nucl. Instr. and Meth. A 443 (2000) 164.
[4] A. Bondar, A. Buzulutskov, L. Shekhtman, Nucl. Instr. and Meth. A 481 (2002) 200.
[5] A. Bondar, A. Buzulutskov, L. Shekhtman, V. Snopkov, A. Vasiljev, Preprint Budker INP 2002-15, E-print physics/0204054.
[6] A. Buzulutskov, Nucl. Instr. and Meth. A 494 (2002) 148–155.
[7] A. Breskin, A. Buzulutskov, R. Chechik, B.K. Singh, A. Bondar, L. Shekhtman, Nucl. Instr. and Meth. A 478 (2002) 225.
[8] F.A. Fraga, et al., Nucl. Instr. and Meth. A 478 (2002) 357.
[9] E. Tsyganov, A. Buzulutskov, P. Antich, J. Moore, R. Parkey, E. Richer, S. Seliounine, N. Slavine, T. Nguyen, in: IEEE Nuclear Science Symposium and MIC-2002 Conference Record, Paper PID 8627, Norfolk, VA, 2002.
[10] A. Bressan, R. de Oliveira, A. Gandi, J.C. Labbe, L. Ropelewski, F. Sauli, D. Mormann, T. Muller, H.J. Simonis, Nucl. Instr. and Meth. A 425 (1999) 254.
[11] A. Bressan, J.C. Labbé, P. Pagano, L. Ropelewski, F. Sauli, Nucl. Instr. and Meth. A 425 (1999) 262.
[12] A. Bondar, A. Buzulutskov, F. Sauli, L. Shekhtman, Nucl. Instr. and Meth. A 419 (1998) 418.
[13] F. Sauli, CERN 77-09, 3 May 1977.
[14] T. Meinschad, L. Ropelewski, F. Sauli, Nucl. Instr. and Meth. A 547 (2005) 342.
[15] S. Agostinelli, et al., Nucl. Instr. and Meth. A 506 (2003) 250.
[16] PENELOPE—a code system for Monte Carlo simulation of electron and photon transport, in: Workshop Proceedings Issy-les-Moulineaux, France, 5–7 November 2001, AEN-NEA.
[17] A. Mantero, B. Mascialino, M.G. Pia, S. Saliceti, P. Nieminen, in: American Nuclear Society Topical Meeting in Monte Carlo, Chattanooga, TN, 2005.
[18] R. Bellazzini, et al., Nucl. Instr. and Meth. A 576 (2007) 183.